Inorganic Chemistry

Article

pubs.acs.org/IC

A Supramolecular Double Sulfate Salt with a Lamellar Type: Crystal Structure and Thermal Behavior

Omar Kammoun,[†,‡] Thierry Bataille,*[,†] Anita Lucas,[†] Vincent Dorcet,[†] Isabelle Marlart,[†] Walid Rekik,[‡] Houcine Naïli,[‡] and Tahar Mhiri[‡]

[†]Institut des Sciences Chimiques de Rennes (UMR 6226), UEB, Université de Rennes 1-CNRS, 263 avenue du Général Leclerc, F-35042 Rennes Cedex, France

[‡]Laboratoire Physicochimie de l'Etat Solide, Département de Chimie, Faculté des Sciences de Sfax, Université de Sfax, BP 1171, 3000 Sfax, Tunisia

Supporting Information

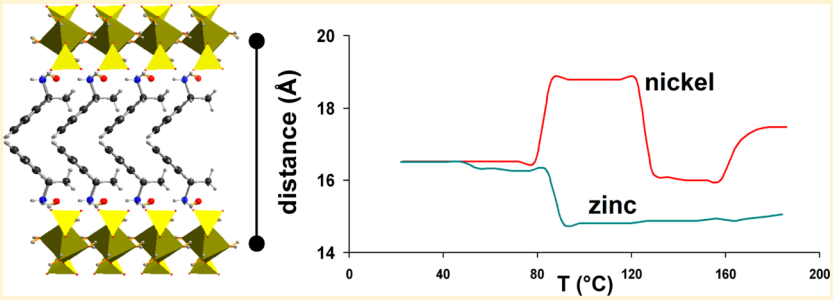

ABSTRACT: The synthesis of a series of supramolecular double sulfate salts using transition metals and the aromatic amine α-methylbenzylamine afforded an unexpected hybrid lamellar structure type. $(C_8H_{12}N)_2[M(H_2O)_4(SO_4)_2]\cdot 2H_2O$ (M = Fe to Zn) crystallizes with a monoclinic structure (S.G. $P2_1/n$), with a significant interlamellar distance of more than 16 Å. While comparable to common clay materials, the crystal structure is actually supramolecular; in particular, the mineral layer is built from hydrogen bonds only. The interlayer space is filled with aromatic amines that form chains through C−H···π interactions. The thermal study of all metal compounds revealed good stability of the filled compounds up to 200 °C. The dehydration proceeds differently according to the metal incorporated into the structure. In particular, the stepped release of water drastically modifies the interlayer space, which is able to vary from 14.8 to 18.8 Å, in an opposite way for the Zn-related compound compared to other metals.

INTRODUCTION

Hybrid organic−inorganic materials have been the subject of major interest in the two last decades, providing a wide range of potential applications from complementary properties of the components that belong to the material.[1−5]

A particular use of amines, generally protonated, as the organic part has provided many types of materials from the beginning of this century. Most articles describe the templating role of the protonated amines,[6−8] whereas a few highlight their importance in several applications, such as optics and catalysis.[9−11] In almost all of these materials, the amine cations interact with the inorganic part through weak hydrogen bonds, so that such compounds belong to Class I of hybrids.

Among them, many sulfates have been elaborated using organic molecules as templates, while cations involved in their syntheses have included transition metals,[12] lanthanides,[13] and actinides.[14] An interesting feature of sulfate-based phases is the diversity of structure framework dimensionality that could be reached, as structures are built from chains, layers, or three-dimensional connections. More recent results on amine metal sulfates actually uncovered their potential applications, from the renewal of zero-dimensional structures belonging to alums and Tutton's salts.[15−17] Indeed, similar double salts were known to show phase transitions at low temperatures, and a few could exhibit interesting properties, such as ferroelectricity[18] or optical properties.[19] Not only are sulfates involved in these features, but recently hybrid halogen-based materials have demonstrated exciting properties.[20−22] Regarding sulfate-based double salts, we demonstrated the ability of some phases to possess order/disorder crystal structure phase transitions, associated with dielectric properties, ca. or above room temperature.[23−25] However, it seems that there is no relationship between the nature of the transition metal and the existence of the dielectric property. A few authors[26] proposed that the amine group may have an influence on such a property.

In the present study, the foremost idea has been to show the influence of aromaticity and/or delocalization of electrons onto the amine on expected dielectric properties. The peculiarity of

Received: December 3, 2013
Published: February 17, 2014

   dx.doi.org/10.1021/ic402974k | Inorg. Chem. 2014, 53, 2619−2627

Table 1. Details of the Synthetic Molar Ratio and Obtained Crystals

compound	FeMBA	CoMBA	NiMBA	CuMBA	ZnMBA
metal/amine/H_2SO_4 molar ratio	1/4/1.8	1/3/1.2	3/3/1.2	1/2/1.2	1/2/1.2
metal concentration (mmol mL^{-1})	0.155	0.155	0.465	0.155	0.155
single crystal color	pale yellow	red	green	blue	colorless

the used α-methylbenzylamine, $C_8H_{11}N$, is that its conformation can be described as a hydrophobic aromatic ring well separated from a hydrophilic monoamine part that accepts hydrogen bonding, by the presence of one aliphatic C atom. This shape would allow separating the contribution of the aromaticity to that of the metal, in the case of dielectric behavior. Instead, the synthetic reactions with this amine provided, while still supramolecular, a new structure type, which can readily be related to layered materials. We recently showed that zinc-based sulfates with aromatic amines, including methylbenzylamine for which a short structure description was given, possess a catalytic activity toward a diastereoselective separation through the nitroaldol reaction.[27]

Lamellar materials are of huge importance in the host−guest chemistry, due to their essential role in intercalation/deintercalation processes, which makes them useful in adsorption, electronic/ionic conduction, and catalysis reactions, for example.[28−30] They include a large variety of materials, from clays,[31] chalcogenides,[32] oxides and oxoanion-based compounds,[33] layered double hydroxides,[34] graphene-based structures,[35] organically pillared clays,[36] or two-dimensional (2D) coordination polymers.[37] They may be pure inorganic, hybrid organic−inorganic, or metal−organic compounds. Their structures are built from at least the propagation of high crystal bonding energy in one lattice direction, that is, covalent or ionic bonds. To our knowledge, the family of compounds described in this study is the first example of layered compounds built from inorganic sheets that possesses a crystal structure consisting of weak interactions only in the three dimensions. For this reason, the crystal structure of members of $(C_8H_{12}N)_2[M(H_2O)_4(SO_4)_2]\cdot 2H_2O$ is described in detail. As the thermal stability of layers into 2D materials has been the key point of potential applications,[38,39] we performed a fine study of the thermal behavior of all the materials. The structural evolution, related to the departure of water, is also presented in the paper.

EXPERIMENTAL SECTION

Materials. $FeSO_4\cdot 7H_2O$ (Merck), $CoSO_4\cdot 6H_2O$ (Prolabo), $NiSO_4\cdot 6H_2O$ (Aldrich Chemie), $CuSO_4\cdot 5H_2O$ (Acros Organics), $ZnSO_4\cdot 7H_2O$ (Carlo, Erba), 1-phenylethanamine (methylbenzylamine $C_8H_{11}N$) (Sigma Aldrich), and H_2SO_4 (97%, Aldrich) were acquired from commercial sources and used as received.

Synthesis. The compounds $(C_8H_{12}N)_2[M(SO_4)_2(H_2O)_4](H_2O)_2$ are obtained by slow evaporation at room temperature. Metal sulfates and methylbenzylamine (MBA) were dissolved together in 10 mL of water and sulfuric acid (pH ≈ 3) with appropriate molar ratios indicated in Table 1. The clear solutions were stirred for ∼15 min until the complete dissolution and were allowed to stand at room temperature. Single crystals in the form of sticks appeared after a few days. Then, the products were filtered off and washed with a small amount of distilled water. For convenience, the final products of formula $(C_8H_{12}N)_2[M(SO_4)_2(H_2O)_4](H_2O)_2$ are named FeMBA, CoMBA, NiMBA, CuMBA, and ZnMBA, following their containing transition metal element.

According to the molar ratio used in the different solutions, the final stoichiometry could be reached directly from the correct metal/amine molar ratio in the case of copper and zinc compounds, that is, 1 to 2. For Co and Fe compounds, it was necessary to increase the excess of amine to reach the final composition. Surprisingly, NiMBA crystals could only be obtained with an equimolar ratio of metal and amine, at a higher concentration.

Single-Crystal Data Collection and Structure Determination. A suitable crystal was glued to a glass fiber mounted on APEX II area detector 4-circles diffractometer. Intensity data sets were collected using Mo Kα radiation (0.71073 Å) through the Bruker AXS APEX2 Sofware Suite. The crystal structure was solved in the monoclinic symmetry, space group $P2_1/n$ (No. 15). Metal and sulfur atoms were located using the direct methods with the program SIR97.[40] C, N, and O atoms from the amine and sulfate groups, and water molecules including H atoms were found from successive difference Fourier calculations using SHELXL-97.[41] Their positions were validated from geometrical considerations as well as from the examination of possible hydrogen bonds. Within a water molecule, the O−H distance was restrained to 0.96(2) Å and the H−H distance to 1.50(3) Å, so that the H−O−H angle fitted the ideal value of 105°. The atomic displacement parameters of the H atoms were fixed at $1.5U_{eq}$ of their parent atom. Structure refinements were performed on F^2 with SHELXL-97. Crystallographic data are given in Table 2.

Thermal Analyses. Temperature-dependent X-ray powder diffraction (TDXD) was carried out with a $\theta-\theta$ Bruker AXS D8 Advance powder diffractometer, equipped with a high-temperature Anton Paar HTK1200 oven camera and a LynxEye detector. Powder patterns were collected sequentially upon heating at 21.6 °C h^{-1} up to 400 °C, with the monochromatized Cu Kα_1 radiation (λ = 1.5406 Å). To ensure satisfactory counting statistics, counting times of 20 min/pattern were selected for the thermal decomposition of the precursors, so that any pattern could be collected within a temperature range of 7.2 °C.

TGA measurements were performed with a Rigaku Thermoflex instrument in flowing air for any compounds, with a heating rate of 10 °C h^{-1} up to 600 °C. For the Ni phase, an additional TGA/DSC measurement was performed under oxygen with a Labsys 1600 (Setaram), in the range 18−600 °C, with a heating rate of 0.5 °C min^{-1}. During this thermal analysis, emitted gases were analyzed using a mass spectrometer (OmniStar, Pfeiffer).

Infrared Studies. Fourier transformed infrared spectroscopy (FTIR) (Bruker Equinox 55) was used to highlight the structural analysis. FTIR studies were performed on 1 mg of material mixed with 100 mg of dried KBr.

RESULTS AND DISCUSSION

Infrared Spectra. Table 3 represents the major selected absorptions in the IR spectra of NiMBA (Figure 1a) and ZnMBA (Figure 1b) compounds with their respective assignments. The presence of α-methylbenzylammonium[42] was evidenced by the appearance of the typical absorptions bands for bending of the NH_3^+ group at ∼1500 cm^{-1}, deformation of CH_3 at 1396 cm^{-1}, deformation of C−H at 700 cm^{-1}, and stretching of the C−C ring at 1461 cm^{-1}. The bending vibration of the water molecules appeared at 1654 cm^{-1}. The presence of SO_4 groups was shown by characteristic band in the lower wavelengths at 558 and 632 cm^{-1}.[43]

Crystal Structure. All of these $(C_8H_{12}N)_2[M(SO_4)_2(H_2O)_4](H_2O)_2$ (M = Fe, Co, Ni, Cu, Zn) compounds are isostructural and crystallize in the monoclinic symmetry, with the centrosymmetric space group $P2_1/n$. The crystal structure is built from inorganic anionic layers of $[M(H_2O)_4(SO_4)_2]^{2-}$

dx.doi.org/10.1021/ic402974k | Inorg. Chem. 2014, 53, 2619−2627

Table 2. Crystal Data and Structure Refinement Details for $(C_8H_{12}N)_2[M(SO_4)_2(H_2O)_4](H_2O)_2$

	(CuMBA)	(NiMBA)	(CoMBA)	(FeMBA)
empirical formula	$C_{16}H_{36}N_2CuO_{14}S_2$	$C_{16}H_{36}N_2NiO_{14}S_2$	$C_{16}H_{36}N_2CoO_{14}S_2$	$C_{16}H_{36}N_2FeO_{14}S_2$
formula	$(C_8H_{12}N)_2[Cu(H_2O)_4(SO_4)_2](H_2O)_2$	$(C_8H_{12}N)_2[Ni(H_2O)_4(SO_4)_2](H_2O)_2$	$(C_8H_{12}N)_2[Co(H_2O)_4(SO_4)_2](H_2O)_2$	$(C_8H_{12}N)_2[Fe(H_2O)_4(SO_4)_2](H_2O)_2$
formula weight	608.12	603.30	603.52	600.44
temperature (K)	150	150	150	150
crystal system	monoclinic	monoclinic	monoclinic	monoclinic
space group	$P2_1/n$	$P2_1/n$	$P2_1/n$	$P2_1/n$
a (Å)	6.226(2)	6.1582(1)	6.1876(2)	6.2172(1)
b (Å)	33.095(1)	32.4154(6)	32.4166(11)	32.5008(7)
c (Å)	7.003(2)	6.9909(1)	7.0025(2)	7.0022(1)
α (deg)	90	90	90	90
β (deg)	109.68(2)	108.4391(6)	108.3530(10)	108.1857(9)
γ (deg)	90	90	90	90
V (Å^3)	1358.7(1)	1323.88(4)	1333.12(7)	1344.22(4)
Z	2	2	2	2
ρ_{cal} (g cm^{-1})	1.486	1.513	1.503	1.483
crystal size (mm^3)	0.4 × 0.15 × 0.1	0.36 × 0.12 × 0.07	0.58 × 0.19 × 0.14	0.18 × 0.06 × 0.05
habit color	blue	green	red	pale yellow
μ (mm^{-1})	1.022	0.957	0.866	0.782
θ range (deg)	θ_{max} = 27.48, θ_{min} = 3.53	θ_{max} = 27.47, θ_{min} = 2.51	θ_{max} = 27.51, θ_{min} = 2.51	θ_{max} = 27.43, θ_{min} = 2.51
index ranges	$h = -8 \rightarrow 7$, $k = -37 \rightarrow 42$, $l = -9 \rightarrow 8$	$h = -7 \rightarrow 7$, $k = -42 \rightarrow 41$, $l = -6 \rightarrow 9$	$h = -5 \rightarrow 7$, $k = -42 \rightarrow 42$, $l = -9 \rightarrow 8$	$h = -6 \rightarrow 8$, $k = -42 \rightarrow 37$, $l = -9 \rightarrow 9$
unique data	3046	3008	3012	3051
observed data [$I > 2\sigma(I)$]	2389	2725	2746	2777
$F(000)$	638	636	634	632
R_1	0.067	0.035	0.0582	0.0336
wR_2	0.090	0.097	0.1775	0.0854
GOF	1.175	1.176	1.204	1.079
no. param	138	188	174	200
transmission factors	T_{min} = 0.658, T_{max} = 0.903	T_{min}= 0.6735, T_{max}= 0.7456	T_{min}= 0.6799, T_{max}= 0.7456	T_{min}= 0.6679, T_{max}= 0.7456
largest difference map hole and peak (e Å^{-3})	$\Delta\rho_{min}$ = −0.46, $\Delta\rho_{max}$ = 0.36	$\Delta\rho_{min}$ = −0.543, $\Delta\rho_{max}$ = 0.576	$\Delta\rho_{min}$ = −0.438, $\Delta\rho_{max}$ = 2.029	$\Delta\rho_{min}$ = −0.355, $\Delta\rho_{max}$ = 0.455

dx.doi.org/10.1021/ic402974k | Inorg. Chem. 2014, 53, 2619−2627

Table 3. Assignments of the Bands of the Infrared Absorption Spectra for Ni- and Zn-Related $(C_8H_{12}N)_2[M(SO_4)_2(H_2O)_4](H_2O)_2$

NiMBA	ZnMBA	vibrational mode assignement
540	541	asymmetry bending of SO_4 group
632	621	
695	699	C−H out of plane deformation mode
921	921	CH_2 rocking mode
985	988	C−C stretching mode
1090	1051	in plan C−H deformation mode
1115	1079	
1153	1127	
1231	1228	
1295		CH_3 deformation mode
	1319	NH_3^+ rocking mode
1370		CH_3 symmetric deformation mode
1455	1392	C−C ring stretching
1506	1482	
1601	1500	
1617	1645	NH_3^+ symmetric bending mode
2921	2929	antisymmetric CH_2 stretch
3005	3023	aromatic CH
	3064	
3498	3430	the stretching vibrations of water molecule

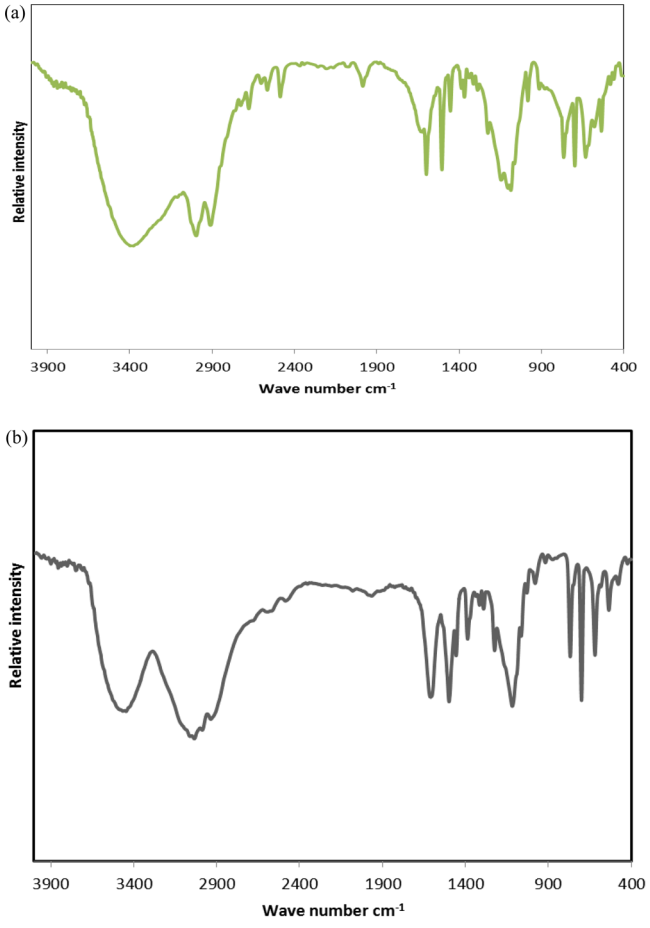

Figure 1. Infrared absorption spectra of (a) Ni and (b) Zn compounds in the region of sulfate anion, benzylammonium cation, and water.

stacking along the crystallographic *b* axis, in between there are methylbenzylammonium $(C_8H_{12}N)^+$ cations, which are located in such a way to compensate for the negative charges of the inorganic part. In addition, free water molecules (OW3) are located on either side of the inorganic sheet and point toward the ammonium cations (Figure 2).

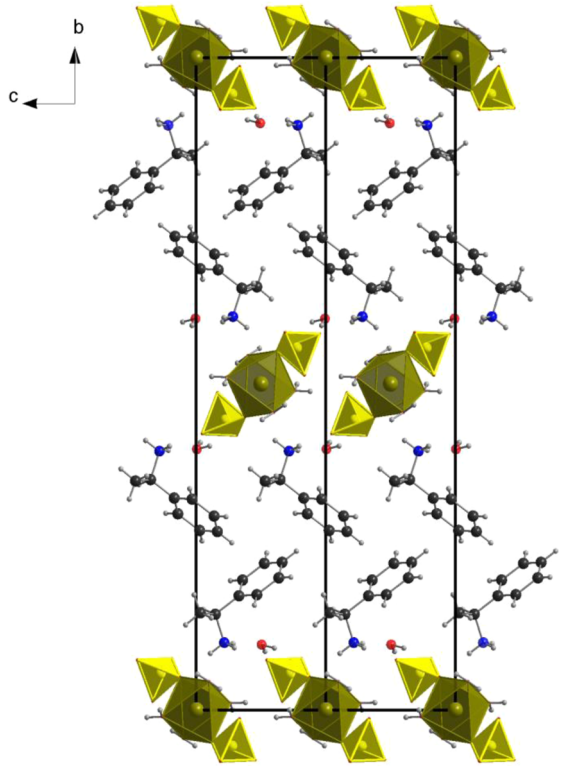

Figure 2. Projection of the structure along the crystallographic *a* axis, showing the lamellar character and the stacking along the *b* axis.

A so-called "inorganic layer" is actually developed from trimeric units, which correspond to one metal octahedron linked to two sulfate tetrahedra. Water molecules (that have already bonded with a metal) can only be connected to sulfates of adjacent trimers through a strong OW−H···O hydrogen bond. It gives rise to a pseudo 2D inorganic sheet parallel to the (*a*, *c*) plane (Figure 3). Such connectivity within the layer definitely gives a strong supramolecular character of the structure.

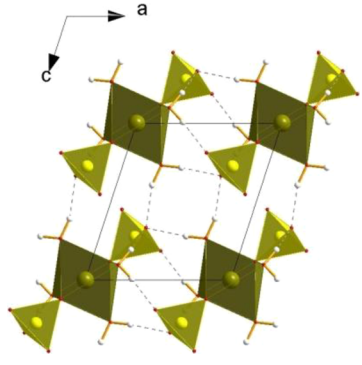

Figure 3. The weak hydrogen bonding between the $[M^{II}(H_2O)_4(SO_4)_2]^{2-}$ entities within the mineral layer, showing its supramolecular aspect.

dx.doi.org/10.1021/ic402974k | Inorg. Chem. 2014, 53, 2619−2627

Because of the steric hindrance of the organic part, combined with the free water molecule, the distance between the mean planes of two adjacent inorganic layers is remarkably high. Indeed, it corresponds to half the value of the *b* unit cell parameter, that is, which is greater than 16.2 Å (see Table 2).

As regarding the supramolecular aspect of the inorganic layer, it is clearly assumed that these compounds define a new supramolecular structure type with a lamellar character, in the sulfate families and their derivatives. To our knowledge, it is the first time that a supramolecular hybrid organic−inorganic compound exhibits a very important distance between inorganic layers. For example, an adeninium oxalate copper complex has been described considering anionic and cationic layers, with a distance between two inorganic sheets of ∼11.4 Å, the anionic layer being built with hybrid supramolecular entities.[44] More important, interlamellar spacing is observed in 2D structures in which layers are built from condensed entities, that is, with ionic or covalent bonds. For example, the most important interlayer distance in sulfates possessing anionic sheets was reached for $La_2(H_2O)_2(C_4H_{12}N_2)(SO_4)_4$,[45] that is, 13.4 Å. Distances beyond 16 Å can be observed mainly in lamellar structures that are readily delaminated, such as in clay materials.[46,47]

The entire structure is then stabilized by O−H···O hydrogen bonding between inorganic entities, N−H···O hydrogen bonding between the inorganic and organic moieties and C−H···π interactions between the aromatic rings of the organic moieties themselves. Indeed, the organic cations are linked together through the aromatic−aromatic interaction between benzene rings in a perpendicular arrangement to form a T-shaped configuration.[48] In the iron-based compound (Figure 4), the value of the angle between two T-shaped aromatic rings

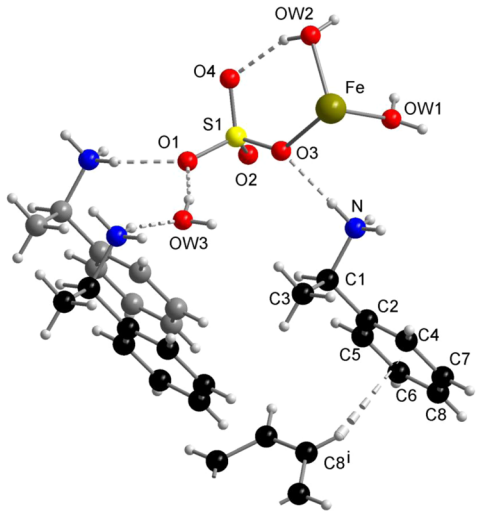

Figure 4. Complete weak interaction network between the chemical entities in part of the structure. Symmetry code: (i) 1 + *x*, *y*, *z*.

is 83.98(8)° and the centroid to centroid distance is 5.0274(1) Å, which is close enough to enable two C−H···π interactions to occur with a distance of about 2.96 Å from C8. Within a molecule, the C−N and C−C distances are close to the usual values observed in others homologous derivates. Each organic cation engages its hydrogen atoms of the ammonium group in N−H···O hydrogen bonds, that is, toward two sulfate oxygen atoms and the free water molecule, so it participates in the stabilization of the structure with the inorganic layers.

The main role of the free water molecule (namely, OW3 in Figure 3) can be seen as a bridge between the ammonium fragment of the organic molecule and the sulfate tetrahedron, as a direct H bond between the latter is not possible for distance purposes.

The transition metal occupies a special position at the center of symmetry of space group $P2_1/n$ and is located in an almost regular octahedron, except Cu. Within the copper octahedron, the Cu−OW2 and Cu−OW3 distances are 1.982 and 1.975 Å, respectively, while the Cu−O3 distance (2.314 Å) is strongly elongated. Thus, the Cu^{2+} ion displays the so-called (4 + 2) coordination type that are often been observed and is consistent with the well-known Jahn−Teller effect.[49,50] This significant Cu−O3 elongation (i.e., more than 0.3 Å) is the origin of the larger interlayer distance between two inorganic layers, compared to the other compounds. Indeed, the organic molecule develops an H-bond between N and the sulfate oxygen O3 which is directly involved in the Cu−O elongation (Figure 3). This is the consequence of the larger value of the *b* cell parameter of the Cu compound (Table 2), which is twice the interlayer distance. On the other hand, the regularity of the metallic octahedral environment in the others explains that the interlayer distances are similar.

Within a layer, the $[M(H_2O)_4(SO_4)_2]^{2-}$ trimeric units are separated from one another with the shortest metal−metal distances ranging between 6.1582(1) Å in NiMBA and 6.2452(2) Å in CoMBA. It is noticeable that such distances are remarkably shorter than these observed in related sulfate compounds exhibiting the same connectivity between the same $[M(H_2O)_4(SO_4)_2]^{2-}$ units, that is, Mg···Mg = 6.785 Å and Co···Co = 6.803 Å in $(C_2H_{10}N_2)[Mg(H_2O)_4(SO_4)_2]$ and $(C_2H_{10}N_2)[Co(H_2O)_4(SO_4)_2]$, respectively.[51,52]

Thermal Decomposition. The importance of both the lamellar feature and the supramolecular structure of the pristine compounds justifies a thorough study of their thermal stability. Indeed, for practical use, efficient materials operate at moderate temperatures, typically, below or around 100 °C for environmentally friendly processes to produce fine chemicals,[53,54] or for adsorption and ion-exchange.[55]

All compounds were individually studied by following their thermal decomposition using in situ X-ray powder diffraction and thermogravimetric analyses. It is known, independent of the isotypical crystal structures, that the thermal behaviors may differ according to the metal incorporated in the structure.[56,57] In the present study, the thermal dehydration of $(C_8H_{12}N)_2[M^{II}(SO_4)_2(H_2O)_4](H_2O)_2$ is similar for all but the Zn-based compound, while the full decompositions into metal sulfates process through a complex scheme which is comparable for all the phases.

Thermal Dehydration of the Nickel-Based Compound (NiMBA) and Related Phases (Fe, Co, Cu). The TG curve and the three-dimensional representation of the powder diffraction patterns obtained during the decomposition of $(C_8H_{12}N)_2[Ni(SO_4)_2(H_2O)_4](H_2O)_2$ are shown in Figures 5a and 6a, respectively. The rapid weight loss (13.5%) observed on TG curve between 50 and ∼90 °C is attributed to the departure of 4.5 water molecules (calculated weight loss, 13.43%). On the TDXD plot, $(C_8H_{12}N)_2Ni(SO_4)_2(H_2O)_{1.5}$ is observed at ∼75 °C. The second weight loss observed on the TG curve between 100 and 150 °C is attributed to the departure of the remaining 1.5 water molecules (total observed weight loss, 18.6%; theoretical weight loss, 17.91%). This led to the formation of the poorly crystallized anhydrous compound, as shown in the

dx.doi.org/10.1021/ic402974k | Inorg. Chem. 2014, 53, 2619−2627

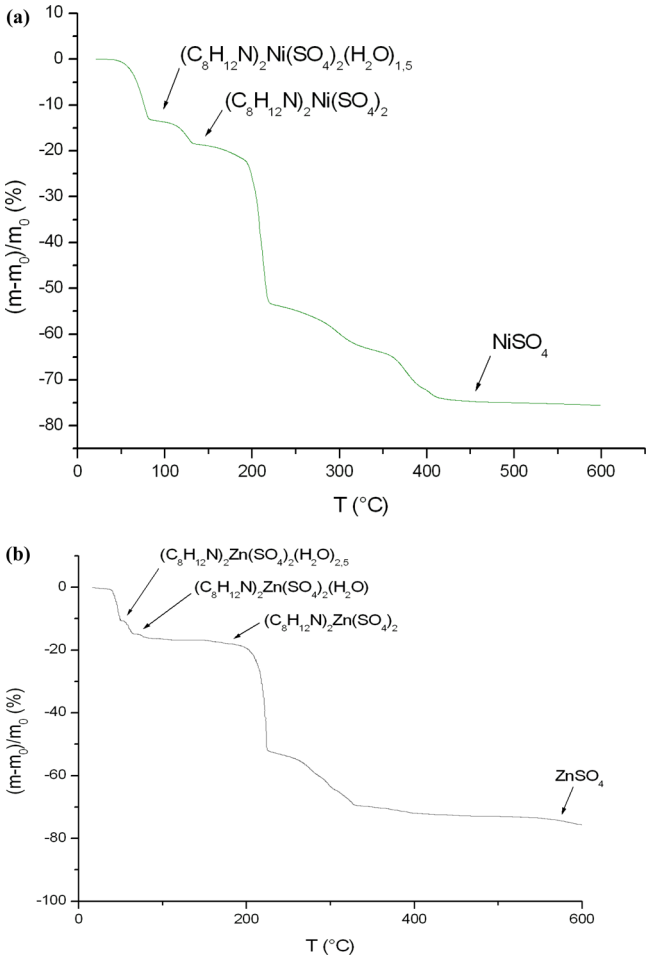

Figure 5. TG curve for the decomposition of $(C_8H_{12}N)_2[M(SO_4)_2(H_2O)_4](H_2O)_2$ in air for (a) Ni and (b) Zn.

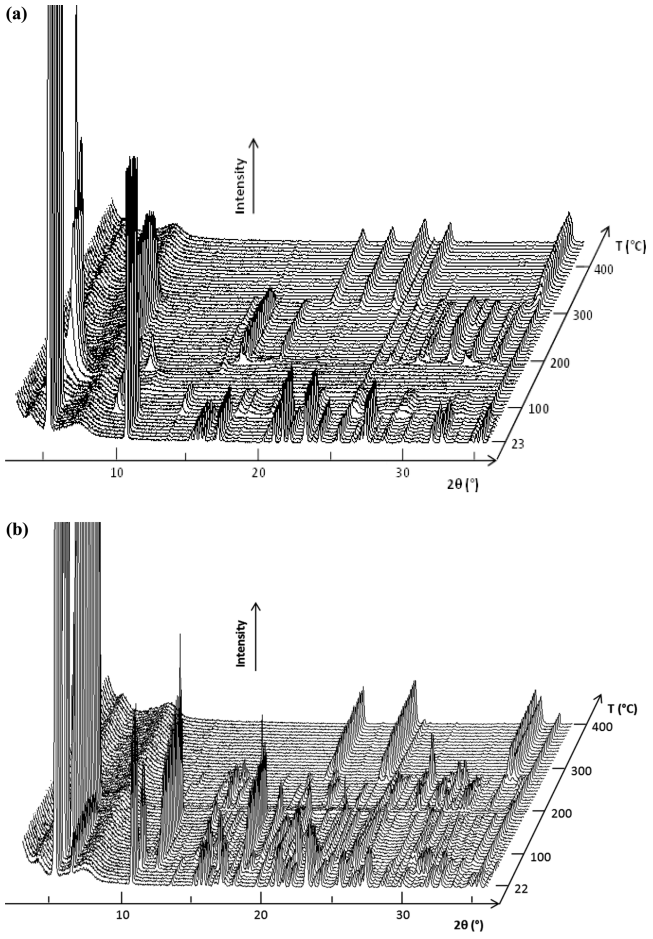

Figure 6. TDXD plot for the decomposition of the compounds in air, showing the successive crystalline phases up to MSO_4 for (a) Ni and (b) Zn.

TDXD plot between 140 and 160 °C. At 180 °C, there is a significant modification of the powder patterns into a phase that is stable up to the beginning of the amine decomposition at ca. 180 °C, while no weight loss is observed. A probable hypothesis would arise in a rearrangement of the nickel polyhedron, as observed elsewhere[58,59] and as discussed below (see Structural Evolution of the Lamellar Phases upon Dehydration).

The same dehydration scheme has been observed for the related phases based on Fe, Co, and Cu metals, for which the transformations differ only in terms of stage temperatures (Table S1, Supporting Information) and crystallinity.

Dehydration of the Zinc-Based Compound (ZnMBA). Both the TG curve and the TDXD plot of the zinc compound are shown in Figures 5b and 6b, respectively. The first weight loss of 9.9% between 30 and 50 °C corresponds to the departure of 3.5 water molecules (theoretical weight loss, 10.3%). The second stage on the dehydration takes place between 55 and 70 °C and corresponds to the departure of 1.5 water molecules (observed weight loss, 14.5%; calculated weight loss, 14.8%). Then, the slower departure of the remaining water molecule is shown between 70 and ca. 105 °C (observed weight loss 16.6%; calculated weight loss 16.2%) and gives rise to the anhydrous compound $(C_8H_{12}N)_2Zn(SO_4)_2$. All weight losses are accompanied with the change of diffraction patterns in Figure 6b, which indicates structure transformations as in the Ni-based compound. The main difference is the formation of a $2.5H_2O$ intermediate of the Zn phase, instead of $1.5H_2O$ for the Ni phase. Similarly, $(C_8H_{12}N)_2Zn(SO_4)_2$ is stable up to ~195 °C, but only slight and continuous modifications in the diffraction patterns are observed within its stability temperature range, in place of the abrupt structural change for the anhydrous nickel phase.

Structural Evolution of the Lamellar Phases upon Dehydration. The layered character of the structures is, as generally observed for lamellar materials, associated with an intense diffraction peak at low angles, arising from preferred orientation of the crystallites. In the present structure, this awaited first peak is correlated to the distance between two inorganic sheets, that is, ~16.2 Å, and corresponds to the (020) reflection. According to the TDXD plots (Figure 6a,b), this most intense diffraction line is observed all along the dehydration stage up to the decomposition temperature (~200 °C), but its angular position varies according to the phases transitions and the thermal evolution. The low quality of the powder diffraction patterns obtained upon dehydration do not allow reaching the values of the *a* and *c* cell parameters, which would give information on the behavior of the inorganic layer itself. Despite weak hydrogen bonding interactions within the inorganic layer, the lamellar character of the structure is then preserved during the dehydration. The variation of the inorganic interlayer distance as a function of temperature for the Zn- and Ni-related compounds is shown in Figure 7. It is seen that the first stage of the dehydration of the Zn compound (into the hemipentahydrate phase) has a negligible impact on

dx.doi.org/10.1021/ic402974k | Inorg. Chem. 2014, 53, 2619−2627

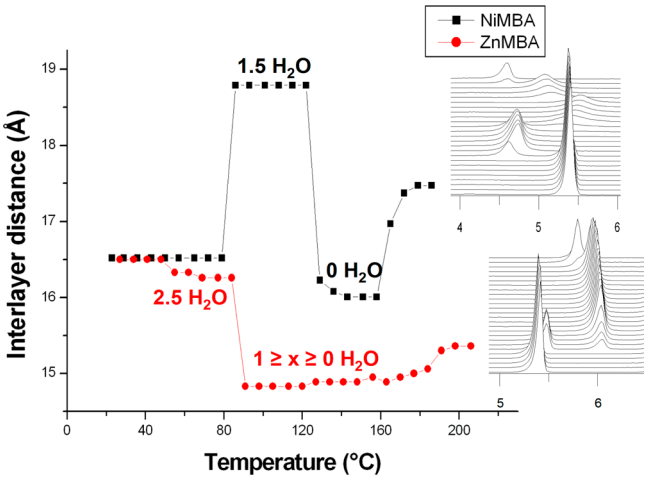

Figure 7. Evolution of the interlayer distance in the structure of the Ni- and Zn-based compounds, according to their different dehydration behavior. The onsets represent the displacement of the first diffraction line (interlayer basal peak), each pattern representing a point in the curve.

the interlayer distance, as it slightly decreases about 0.2 Å. As it was supposed that the free water molecule (so-called OW3 in the precursor) is a bridge between the amine and the inorganic layer, it is expected that this water molecule keeps its role. In fact, water molecules connected to the Zn cation (namely, Ow1 and Ow2) can easily be released, as a rearrangement of the Zn polyhedron from the octahedron to a tetrahedron is still possible, thus incorporating more sulfate oxygen atoms. This is due to the electronic configuration d^{10} of Zn^{2+}, which equally favors octahedral and tetrahedral environments in terms of crystal field stabilization energy. Among many double sulfate salts involving 3d transition metal cations, there is a unique crystal structure in which the metal, a zinc atom, adopts a tetrahedral coordination, that is, $Zn[C(NH_2)_3]_2(SO_4)_2$.[60] No other existing double alkaline/amine metal sulfate salts possesses a tetrahedrally coordinated metal atom, even in the guanidinium-based sulfate family.[15]

At ~90 °C, there is a dramatic increase in the distance for the Ni—and related phases—of more than 2 Å, while it decreases about 2 Å for the Zn phase. According to the number of water molecules in the formula of the Zn compound from this temperature (i.e., less than $1H_2O$), it is obvious that the expected free remaining molecules are released. The consequence would be that the ammonium groups come closer to the inorganic layers to ensure the connectivity through the H-bonds, thus decreasing the interlayer space. In the same manner, the release of the free water molecule is expected for the Ni compound at this temperature. However this stage implies the departure of $4.5H_2O$ per formula, which also involves the release of some water molecules bonded to Ni. Contrary to Zn^{2+}, a tetrahedral environment for a non d^5 or d^{10} cation (i.e., Fe, Co, Ni, Cu) should not be favorable. Figure S1, Supporting Information illustrates the behavior of the inorganic interlayer distance for Fe-, Co-, and Cu-based compounds, which is clearly similar to that of the Ni-based compound. Despite the fact that Fe^{2+} (d^6) and Co^{2+} (d^7) cations are able to adopt a tetrahedral environment, it is obvious that the crystal field energy does not favor a tetrahedron. Then, the rearrangement around the Ni^{2+} cation clearly differs from the zinc cation, which probably involves a strong modification into the layer itself. It is at the origin of the expansion of the interlayer space instead of its diminution. Up to 200 °C, there is no structural evolution of the Zn phase, and the interlayer distance only slightly increases, certainly due to the thermal expansion of the material. For the Ni-related phase, the departure of the last water molecules at 130 °C leads to the decrease of the distance to about 16 Å. As explained before, another phase transition has been observed at 180 °C on the TDXD plot before the decomposition. This is in agreement with the significant increase of the interlayer space of more than 1.5 Å, while it was not observed in the Zn compound.

Additional in situ measurements were performed for the Ni- and Zn-related compounds, in order to study the stability of all hydrates observed upon heating. Each partially hydrated phase was obtained by reaching their formation temperature, prior to cooling down to room temperature. In all cases, the pristine hexahydrate phase was regenerated rapidly in ambient conditions. It confirms that the metal cation is stabilized by an octahedral environment of water molecules, instead of a tetrahedral environment expected at higher temperatures.

The keeping of the interlayer spacing is explained by the existence of H bonds in all stages of the dehydration. Indeed, it has been shown in terephtalate- and benzoate-intercalated LDH materials (LDH intercalated with aromatic molecules) that the hydrogen bonding is critical in maintaining the stability of the expanded interlayer region.[61] In the cited compounds, the water loss (i.e., the loss of H bonding) leads to a flattening of the organic molecules relative to the layers, which significantly reduces the *d* spacing. On the contrary, the water release in the 2D sulfates, though having an influence on the variation of interlayer space, does not lead to the structure collapse, because of the presence of weak interactions provided by the protonated amines in the vicinity of the mineral layer.

Decomposition of $(C_8H_{12}N)_2M(SO_4)_2$ into metal sulfates. Beyond 200 °C, the layered compounds decompose, as seen in the TG curves (Figure 5a,b). The decomposition is complex and proceeds in several stages. The weight losses associated with the steps could not allow proposing chemical formulas. However, the mass spectrometry (Figure S2, Supporting Information) of the Ni compound showed that the amine group decomposes at the first stage, together with a part of the sulfate groups, at ~200 °C, which corresponds to a rapid and important weight loss. Between 220 and ~300 °C (280 °C for the Zn phase), the weight loss is much slower. The TDXD plots (Figure 6a,b) show crystalline phases in this temperature range. Surprisingly, the small modification of the patterns at about 250 °C did not correspond to a single phase transition but was clearly interpreted as a multiphase transformation (Figure S3, Supporting Information). In addition, for all related materials (from Fe to Zn), these crystallized phases differ from their powder diffraction patterns (Figure S4, Supporting Information). The metal sulfate is then obtained at ~300 °C in all cases and is stable at least up to 600 °C.

CONCLUSION

We have synthesized a series of double sulfate salts of transition metal elements (from Fe to Zn) and α-methylbenzylamine. The typical structural feature observed in many related double salts, that is to say, a supramolecular structure built from isolated entities, has been obtained as it was expected to. The design of the protonated amine, in the form of α-methylbenzylammonium, allowed forming weak hydrogen bonds from the amine group and π interactions from the

dx.doi.org/10.1021/ic402974k | Inorg. Chem. 2014, 53, 2619−2627

aromatic moiety. As a consequence, we have obtained for the first time a supramolecular double salt that possesses a lamellar character, with a significant interlayer distance of more than 16 Å. Furthermore, the study of the thermal dehydration of all the members of the family could establish that the compounds behave like clay and related materials. Indeed, the water release allowed the lamellar character to be preserved, while important variations of the interlayer space have been observed, depending on the nature of the metal. However, there is no structure collapse even for the anhydrous phases.

■ ASSOCIATED CONTENT

Supporting Information

Table of the dehydration stage temperatures for other metal-related compounds, variation of the interlayer distance into the Fe, Co, and Cu compounds, mass spectrometry results for the Ni compound, and powder patterns of nonambient temperature phases and comparison between them. This material is available free of charge via the Internet at http://pubs.acs.org. Crystallographic data for CCDC-961904 (Co), CCDC-961905 (Cu), CCDC-961906 (Fe), CCDC-961907 (Ni) can be obtained free of charge from The Cambridge Crystallographic Data Centre via www.ccdc.cam.ac.uk/data_request/cif.

■ AUTHOR INFORMATION

Corresponding Author

*Fax: +33 02 23 23 67 99. E-mail: thierry.bataille@univ-rennes1.fr.

Notes

The authors declare no competing financial interest.

■ ACKNOWLEDGMENTS

The authors gratefully acknowledge the CNRS, the Ministère de l'Enseignement Supérieur (Tunisia), and the Doctorate School of Chemistry, Université de Rennes 1 for financial support. We want to thank the CDIFX (Centre de Diffractométrie X) − Institut des Sciences Chimiques de Rennes for supplying single-crystal data collection. The authors thank C. Derouet for his assistance in powder data collection and B. Lefeuvre for IR measurements. Miss R. Elson is gratefully acknowledged for her dutiful diligence of maintaining the grammatical structures of this work.

■ REFERENCES

(1) Sanchez, C.; Julián, B.; Belleville, P.; Popall, M. *J. Mater. Chem.* **2005**, *15*, 3559.
(2) Mohana Reddy, A. L.; Gowda, S. R.; Shaijumon, M. M.; Ajayan, P. M. *Adv. Mater.* **2012**, *24*, 5045−64.
(3) Sanchez, C.; Belleville, P. *Chem. Soc. Rev.* **2011**, *40*, 696−753.
(4) Dolbecq, A.; Dumas, E.; Mayer, C. R.; Mialane, P. *Chem. Rev.* **2010**, *110*, 6009−6048.
(5) Rao, C. N. R.; Cheetham, A. K.; Thirumurugan, A. *J. Phys.: Condens. Matter* **2008**, *20*, 083202.
(6) Gérardin, C.; Loiseau, T.; Férey, G.; Taulelle, F.; Navrotsky, A. *Chem. Mater.* **2002**, *14*, 3181−3186.
(7) Yao, H.-B.; Gao, M.-R.; Yu, S.-H. *Nanoscale* **2010**, *2*, 323−334.
(8) Rao, C. N. R.; Natarajan, S.; Choudhury, A.; Neeraj, S.; Ayi, A. A. *Acc. Chem. Res.* **2001**, *34*, 80−87.
(9) Leblanc, N.; Allain, M.; Mercier, N.; Sanguinet, L. *Cryst. Growth Des.* **2011**, *11*, 2064−2069.
(10) Bi, W.; Louvain, N.; Mercier, N.; Luc, J.; Rau, I.; Kajzar, F.; Sahraoui, B. *Adv. Mater.* **2008**, *20*, 1013−1017.
(11) Wight, A. P.; Davis, M. E. *Chem. Rev.* **2002**, *102*, 3589−3613.
(12) Rao, C. N. R.; Behera, J. N.; Dan, M. *Chem. Soc. Rev.* **2006**, *35*, 375−387.
(13) Bataille, T.; Louër, D. *J. Solid State Chem.* **2004**, *177*, 1235−1243.
(14) Norquist, A. J.; Doran, M. B.; O'Hare, D. *Inorg. Chem.* **2005**, *44*, 3837−3843.
(15) Fleck, M.; Bohatý, L.; Tillmanns, E. *Solid State Sci.* **2004**, *6*, 469−477.
(16) Bataille, T. *Acta Crystallogr., Sect. C: Cryst. Struct. Commun.* **2003**, *59*, m459−m461.
(17) Rekik, W.; Naïli, H.; Mhiri, T.; Bataille, T. *Acta Crystallogr., Sect. E: Struct. Rep. Online* **2005**, *61*, m629−m631.
(18) Kirpichnikova, L. F.; Shuvalov, L. A.; Ivanov, N. R.; Prasolov, B. N.; Andreyev, E. F. *Ferroelectrics* **1989**, *96*, 313−317.
(19) Ushasree, P. M.; Jayavel, R.; Subramanian, C.; Ramasamy, P. *J. Cryst. Growth* **1999**, *197*, 216−220.
(20) Wang, G.-E.; Wang, M.-S.; Zhang, M.-J.; Cai, L.-Z.; Liu, B.-W.; Zhang, C.-J.; Guo, G.-C.; Huang, J.-S. *Inorg. Chem. Commun.* **2012**, *23*, 137−141.
(21) Leblanc, N.; Mercier, N.; Zorina, L.; Simonov, S.; Auban-Senzier, P.; Pasquier, C. *J. Am. Chem. Soc.* **2011**, *133*, 14924−14927.
(22) Phanon, D.; Gautier-Luneau, I. *Angew. Chem., Int. Ed. Engl.* **2007**, *46*, 8488−8491.
(23) Naïli, H.; Rekik, W.; Bataille, T.; Mhiri, T. *Polyhedron* **2006**, *25*, 3543−3554.
(24) Yahyaoui, S.; Rekik, W.; Naïli, H.; Mhiri, T.; Bataille, T. *J. Solid State Chem.* **2007**, *180*, 3560−3570.
(25) Hajlaoui, F.; Yahyaoui, S.; Naili, H.; Mhiri, T.; Bataille, T. *Inorg. Chim. Acta* **2010**, *363*, 691−695.
(26) Masse, R.; Zyss, J. Eur. Patent EP0488869B1 1996, 1996/06.
(27) Kammoun, O.; Rekik, W.; Bataille, T.; Mahmudov, K. T.; Kopylovich, M. N.; Naïli, H. *J. Organomet. Chem.* **2013**, *741*−*742*, 136−140.
(28) Centi, G.; Perathoner, S. *Microporous Mesoporous Mater.* **2008**, *107*, 3−15.
(29) Goh, K.-H.; Lim, T.-T.; Dong, Z. *Water Res.* **2008**, *42*, 1343−1368.
(30) Butler, S. Z.; Hollen, S. M.; Cao, L.; Cui, Y.; Gupta, J. A.; Gutie, H. R.; Heinz, T. F.; Hong, S. S.; Huang, J.; Ismach, A. F.; Johnston-halperin, E.; Kuno, M.; Plashnitsa, V. V; Robinson, R. D.; Ruoff, R. S.; Salahuddin, S.; Shan, J.; Shi, L.; Spencer, O. M. G.; Terrones, M.; Windl, W.; Goldberger, J. E. *ACS Nano* **2013**, *7*, 2898−2926.
(31) Nishimura, S.; Takagaki, A.; Ebitani, K. *Green Chem.* **2013**, *15*, 2026−2042.
(32) Deguchi, K.; Takano, Y.; Mizuguchi, Y. *Sci. Technol. Adv. Mater.* **2012**, *13*, 054303.
(33) Kendrick, E.; Slater, P. *Annu. Rep. Sect. "A" (Inorg. Chem.)* **2010**, *106*, 429−457.
(34) Newman, S. P.; Jones, W. *New J. Chem.* **1998**, *22*, 105−115.
(35) Novoselov, K. S.; Geim, A. K.; Morozov, S. V.; Jiang, D.; Zhang, Y.; Dubonos, S. V.; Crigorieva, I. V.; Firsov, A. A. *Science* **2004**, *306*, 666−669.
(36) Vivani, R.; Alberti, G.; Costantino, F.; Nocchetti, M. *Microporous Mesoporous Mater.* **2008**, *107*, 58−70.
(37) Umeyama, D.; Horike, S.; Inukai, M.; Itakura, T.; Kitagawa, S. *J. Am. Chem. Soc.* **2012**, *134*, 12780−12785.
(38) Xie, W.; Xie, R.; Pan, W.; Hunter, D.; Koene, B.; Tan, L.; Vaia, R. *Chem. Mater.* **2002**, *14*, 4837−4845.
(39) Kim, T. W.; Ha, H.-W.; Paek, M.-J.; Hyun, S.-H.; Baek, I.-H.; Choy, J.-H.; Hwang, S.-J. *J. Phys. Chem. C* **2008**, *112*, 14853−14862.
(40) Altomare, A.; Burla, M. C.; Camalli, M.; Cascarano, G. L.; Giacovazzo, C.; Guagliardi, A.; Moliterni, A. G. G.; Polidori, G.; Spagna, R. *J. Appl. Crystallogr.* **1999**, *32*, 115−119.
(41) Sheldrick, G. M. *Acta Crystallogr., Sect. A: Found. Crystallogr.* **2008**, *64*, 112−122.
(42) Brittain, H. G. *Cryst. Growth Des.* **2011**, *11*, 2500−2509.
(43) Karydis, D. A.; Boghosian, S.; Nielsen, K.; Eriksen, K. M.; Fehrmann, R. *Inorg. Chem.* **2002**, *41*, 2417−2421.

(44) García-Teran, J. P.; Castillo, O.; Luque, A.; García-Couceiro, U.; Beobide, G.; Roman, P. *Inorg. Chem.* **2007**, *46*, 3593−3602.
(45) Bataille, T.; Louër, D. *J. Mater. Chem.* **2002**, *12*, 3487−3493.
(46) Leroux, F.; Taviot-Guého, C. *J. Mater. Chem.* **2005**, *15*, 3628−3642.
(47) Nakamura, T.; Ogawa, M. *Langmuir* **2012**, *28*, 7505−11.
(48) Sinnokrot, M. O.; Valeev, E. F.; Sherrill, C. D. *J. Am. Chem. Soc.* **2002**, *124*, 10887−10893.
(49) Hawthorne, F. C.; Cooper, M. A. *Mineral. Mag.* **2013**, *77*, 2901−2912.
(50) Smirnov, P. R.; Trostin, V. N. *Russ. J. Gen. Chem.* **2009**, *79*, 1591−1599.
(51) Rekik, W.; Naïli, H.; Mhiri, T.; Bataille, T. *Mater. Res. Bull.* **2008**, *43*, 2709−2718.
(52) Rekik, W.; Naïli, H.; Mhiri, T.; Bataille, T. *Solid State Sci.* **2012**, *14*, 1503−1511.
(53) Rodriguez, I.; Climent, M.; Iborra, S.; Fornes, V.; Corma, A. *J. Catal.* **2000**, *192*, 441−447.
(54) Tagusagawa, C.; Takagaki, A.; Hayashi, S.; Domen, K. *J. Am. Chem. Soc.* **2008**, *130*, 7230−7231.
(55) Khan, A. I.; Ragavan, A.; Fong, B.; Markland, C.; O'Brien, M.; Dunbar, T. G.; Williams, G. R.; O'Hare, D. *Ind. Eng. Chem. Res.* **2009**, *48*, 10196−10205.
(56) Nelwamondo, A. N.; Eve, D. J.; Watkins, G. M.; Brown, M. E. *Thermochim. Acta* **1998**, *318*, 165−175.
(57) Yuvaraj, S.; Fan-Yuan, L.; Tsong-Huei, C.; Chuin-Tih, Y. *J. Phys. Chem. B* **2003**, *107*, 1044−1047.
(58) Groust, J.-F.; Pommier, C.; Stievano, L.; Villain, F.; Giorgetti, C.; Baudelet, F.; Massiani, P. *Catal. Lett.* **2005**, *102*, 257−260.
(59) Miller, S. R.; Pearce, G. M.; Wright, P. a; Bonino, F.; Chavan, S.; Bordiga, S.; Margiolaki, I.; Guillou, N.; Férey, G.; Bourrelly, S.; Llewellyn, P. L. *J. Am. Chem. Soc.* **2008**, *130*, 15967−15981.
(60) Morimoto, C. N.; Lingafelter, E. C. *Acta Crystallogr. Sect. B: Struct. Crystallogr. Cryst. Chem.* **1970**, *26*, 335−341.
(61) Vucelic, M.; Moggridge, G. D.; Jones, W. *J. Phys. Chem.* **1995**, *99*, 8328−8337.